Colloids and Surfaces B: Biointerfaces 83 (2011) 1–9

Contents lists available at ScienceDirect

Colloids and Surfaces B: Biointerfaces

journal homepage: www.elsevier.com/locate/colsurfb

Adsorption and bioactivity studies of albumin onto hydroxyapatite surface

Elena Mavropoulos[a,*], Andréa M. Costa[a], Lilian T. Costa[b,c], Carlos A. Achete[b,d], Alexandre Mello[a], José M. Granjeiro[e], Alexandre M. Rossi[a]

[a] Brazilian Center for Physics Research, Xavier Sigaud 150, 22290-180, RJ, Brazil
[b] National Institute of Metrology, Standardization and Industrial Quality, N.S. das Graças 50, Duque de Caxias, CEP 25250-020, RJ, Brazil
[c] Biophysics Institute, Pólo Xérem, UFRJ, Duque de Caxias 25000-000, Brazil
[d] Metallurgical and Materials Engineering, UFRJ, RJ 21945-970, Brazil
[e] Department of Cellular and Molecular Biology, Institute of Biology, UFF, 24050-120 Niterói, RJ, Brazil

ARTICLE INFO

Article history:
Received 2 August 2010
Received in revised form 6 October 2010
Accepted 6 October 2010
Available online 19 October 2010

Keywords:
Hydroxyapatite
Bovine serum albumim
Isotherms
Bioactivity

ABSTRACT

Bovine serum albumin (BSA) may have an inhibitory or promoter effect on hydroxyapatite (HA) nucleation when apatite is precipitated in a medium containing the protein. In this study we evaluated the influence of BSA on the precipitation of calcium phosphate phases (CP) from simulated body fluid (SBF) when the protein was previously bounded to HA surface. The kinetics of BSA immobilization onto hydroxyapatite surface was performed in different buffers and protein concentrations in order to adjust experimental conditions in which BSA was tightly linked to HA surface for long periods in SBF solution. It was shown that for BSA concentration higher than 0.1 mg/mL the adsorption to HA surface followed Langmuir–Freundlich mechanisms, which confirmed the existence of cooperative protein–protein interactions on HA surface. Fourier Transformed Infrared Attenuated Total Reflectance Microscopy (FTIRM-ATR) evidenced changes in BSA conformational state in favor of less-ordered structure. Analyses from high resolution grazing incident X-ray diffraction using synchrotron radiation (GIXRD), Scanning Electron Microscopy (SEM) and Atomic Force Microscopy (AFM) showed that a poorly crystalline calcium phosphate was precipitated on the surface of HA discs coated with BSA, after the immersion in SBF for 4 days. The new bioactive layer had morphological characteristics similar to the one formed on the HA surface without protein. It was identified as a carbonated apatite with preferential crystal growth along apatite 002 direction. The GIXRD results also revealed that BSA layer bound to the surface inhibited the HA dissolution leading to a reduction on the formation of new calcium phosphate phase.

1. Introduction

Albumin is the most abundant protein in the circulatory system, possessing low content of tryptophan and methionine and a high content of cystine and charged amino acids, aspartic and glutamic acids, lysine, and arginine. Its great affinity to hydroxyapatite could be explained by the presence of charged residues that can bind to phosphate and calcium sites on hydroxyapatite surface. The aspartic and glutamic acids residues could bind to calcium site while lysine and arginine could bind to phosphate groups [1].

The proteins adhesion onto biomaterial surface is a key point in bioengineering because of the fundamental role that proteins play in the contact between inorganic surface and a biological environment. For applications involving hard and soft tissues regeneration an excellent adhesion of selected proteins allows, in most cases, a better biocompatibility and a better recovery of the biological function of the implants. In this sense, the protein may play two important roles: the first due to its specific biological activity, the second due to its importance in the processes of biomineralization as inhibiting or promoting [2] the calcium phosphate formation.

In vivo studies support that serum proteins are adsorbed immediately on the surface of HA after implantation and the initial cellular response are dependent on the proteins adsorbed by the implant surfaces [3]. The first protein layer adsorbed on the implant surface affects the cellular adhesion [4,5], differentiation and extracellular matrix production. It also affects dissolution, nucleation and crystal growth of HA [6,7]. Therefore, the kinetic study of protein adsorption onto biomaterials is primordial to understand the nature of interactions between surfaces and proteins and in some cases allow us to assess the arrangement, and the conformation of the proteins onto the biomaterial surface. In general, the protein adsorption occurs in two steps [8]: first, the protein is rapidly adsorbed and forms a strongly bonded denatured monolayer due to a multiple site binding. The proteins of the first monolayer lose their tertiary structure and consequently biological activity. A second protein

* Corresponding author. Tel.: +55 21 2141 7209; fax: +55 21 2141 7160.
E-mail addresses: elenatude@gmail.com, elena@cbpf.br (E. Mavropoulos).

0927-7765
doi:10.1016/j.colsurfb.2010.10.025

layer begins to be formed slowly and leads to a monolayer of non-denaturated with biological activity. Information concerning the surface coverage could be obtained by adsorption isotherms. The Langmuir isotherms have been used to explain the protein monolayer formation on biomaterial surface. However, many factors could also influence the adsorption process such as (i) multiple-site binding for protein, which often results in irreversible adsorption and denaturation, (ii) the heterogeneous nature of most solid surfaces, and (iii) lateral and other cooperative interactions. As a consequence, other models such as Temkin, Langmuir–Freundlich, Bilangmuir, and extended Langmuir (multilayer) have been tested in the recent years [9]. Consequently, is primordial to find out a model that is able to account for these interactions most efficiently in a qualitative as well as a quantitative way.

Concerning the biomineralization process several works suggest that BSA inhibit the hydroxyapatite formation when apatite is precipitated in a medium containing the protein [10,11]. Mueller and Sikes [12] suggested that there are biomineralization inhibitors that affect the nucleation and crystal growth of apatite. In the first case the biomolecules could bind to the ions present in simulated biological fluid by sequestering lattice ions therefore reducing ion activity and inhibiting nucleation. In the second case the biomolecules affect the crystal growth by binding to crystal surfaces rather than ions present in simulated biological fluid. Conversely, Marques et al. [11] increased the carbonate content of simulated inorganic plasma containing BSA (CSIPA) causing a higher mineralization on calcium phosphate ceramics and bioglass substrates when compared with simulated body fluid containing BSA (SBFA).

In general, the effect of albumin on hydroxyapatite crystallization has been studied by the addition of BSA into aqueous media or simulated body fluid containing calcium and phosphate. In these cases the protein is widely dispersed in the medium where apatite crystals are forming. However, few works studied in detail the precipitation of calcium phosphates onto wide surfaces where BSA was previously adsorbed. In this work we investigated the kinetics of BSA adsorption onto apatite surface and the conditions where mono and multilayers of proteins are formed. This study also focused on the characterization of the calcium phosphate layer (CP) precipitated onto HA surface previously coated with a film of BSA, after the immersion in simulated body fluid (SBF) for 7 days. The role of BSA on hydroxyapatite bioactivity is discussed.

2. Materials and methods

Hydroxyapatite (HA) was synthesized via wet method as described elsewhere [13]. The powder was uni-axially pressed at 30 KN into discs with diameter of 10 mm and thickness of 1 mm. These samples were then sintered with a temperature increment of 10 °C s^{-1} until reaching 1000 °C and left during 2 hours at this temperature. Bovine serum albumin (BSA) a well-characterized protein with a molecular weight of 69 kDa, isoelectric point of 4.9 (14) and dimensions of 14.0 nm × 4.0 nm [15] was obtained from the Sigma Chemical Co. (A7638, crystallized and lyophilized). BSA structure contains 70% of α helix and 15% of β sheet [16].

The HA sample had a Ca/P ratio of 1.67 ± 0.03, which was measured by X-Fluorescence and specific surface area of 45 ± 5 m^2 measured by BET method. Conventional X-ray diffraction was used to characterize hydroxyapatite powder samples. For a better understanding of the HA discs, surface samples were characterized by grazing-incidence X-ray diffraction technique (GIXRD) performed with synchrotron radiation operating at the energy of 9000 eV (wavelength of λ = 1.377 Å) fixed incident angle theta = 0.5° and 1.0°, 2 theta in the range of 9–50° at a rate of 0.04°/point/second. This method provided a high photon density and a better pick resolution for the HA surface structural analyses. The GIXRD measurements were performed at the Brazilian Synchrotron Light National Laboratory (LNLS). Fourier Transformed Infrared Attenuated Total Reflectance Microscopy (FTIRM-ATR) studies were performed using a Shimadzu IR- Prestige-21/AIM-880 operating in Attenuated Total Reflectance (ATR) mode from 700 to 4000 cm^{-1}. Surface images of HA disc no-coated (HA) and coated with BSA (HA + BSA) were obtained by SEM (Jeol-JSM-6460 LV) with dispersive energy spectrometer (EDS). Surface topography of HA disc before and after BSA adsorption with different concentrations were performed using a Nanowizard AFM (JPK) operating in intermittent contact with a resonant frequency of ~75 kHz.

3. BSA adsorption isotherms

Adsorption experiments were carried out in a batch system using HA powder and HA discs. Tubes containing 0.1 g of HA (in triplicate) were incubated with BSA (8 mL of solutions from 0 to 2 mg/mL) and moderately shaken for 24 h at 37 °C. Incubation period of 72 h showed no significant difference in the amount of protein adsorbed. A control was set up at the same BSA concentration (without HA) to allow corrections to be made for protein losses in the system. BSA adsorption isotherms were performed using 0.01 M and 0.05 M of phosphate buffer (K_2HPO4/NaOH) and 0.01 M of acetate buffer (acetic acid/NaOH) solutions at pH 6.0. After incubation time, the supernatant obtained was analyzed by UV-Vis spectrometry. The amount of adsorbed protein was calculated from solution depletion. The same experiment described above was performed using HA discs and 0.1 mg/mL BSA. To know the amount of protein that was not effective adsorbed the HA + BSA samples were immediately immersed in phosphate buffer and the suspension was again moderately shaken for 24 hours at 37 °C and analyzed by UV–Vis.

4. In vitro bioactivity test

SBF is an acellular aqueous solution with an ionic composition that closely resembles the human plasma and buffered to physiological pH 7.4 (n-SBF) [17]. The assessment of in vitro bioactivity was carried out by soaking HA and HA + BSA discs (0.1 mg BSA/mL in 0.05 M phosphate buffer) using 15 mL of Hepes-buffered "SBF", maintained at 37 °C in polyethylene tubes. After soaking period of 7 days the discs were removed from the fluid, gently washed with Milli-Q water and dried at 37 °C before characterization. To evaluate surface modification occurred by HA dissolution in aqueous media a control sample was set up in parallel with HA disc immersed in 15 mL of Milli-Q water. Solution aliquots were collected with a micropipette, centrifuged and filtered through a 0.22 μm Durapore membrane (Millipore) with diameter equal to 13 mm. The calcium and phosphorus concentrations of the filtrate were determined by ICP-OES. All experiments were performed in triplicate, by running three parallel independent tubes simultaneously.

5. Results and discussion

5.1. The BSA adsorption onto hydroxyapatite surface

The adsorption of BSA onto HA surface by different protein concentrations in phosphate buffers (0.05 M and 0.01 M) and acetate buffer (0.01 M) are shown in Fig. 1. The adsorption was slightly more efficient on 0.01 M acetate buffer than on 0.01 M phosphate buffer, indicating that the buffer nature has no significant effect on BSA adsorption onto HA surface.

The increase of phosphate concentration from 0.01 to 0.05 M caused a decrease of BSA adsorption by HA surface. This behavior was also observed by Yin et al. [18]. This could be attributed to the

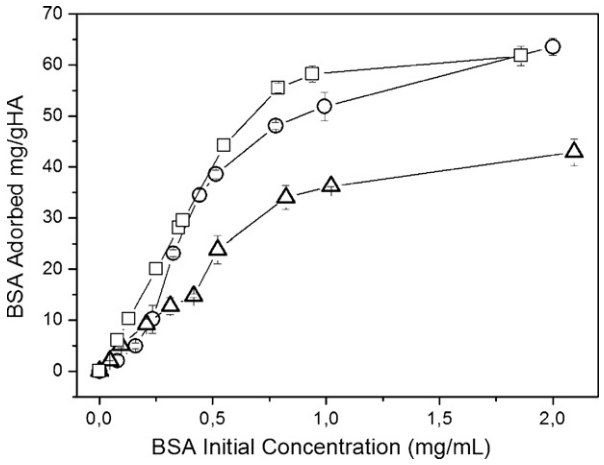

Fig. 1. Isotherms adsorption of BSA on HA powder in different buffers: phosphate 0.01 M (●), phosphate 0.05 M (Δ) and acetate 0.01 M (□).

affinity of phosphate groups for HA calcium sites [19]. Additionally, the increase of phosphate concentration on the aqueous medium lead to more PO_4^{3-} in the diffusion layer of the electric double layer at HA surface resulting in an increase of negative Zeta potential [20]. This effect enhances the electrostatic repulsion force between HA and BSA and could explain the decrease of BSA adsorption for higher phosphate concentration. Independently of the buffer concentration no protein was released from HA surface after 24 hours of desorption experiment at pH = 6.0 and 37 °C.

The adsorption process of BSA onto HA surface was also investigated by fitting the experimental data of Fig. 1 with Langmuir, Freundlich and Langmuir–Freundlich equations. The Langmuir isotherm theoretically supposes that the adsorption takes place on fixed homogenous absorption sites of equal energy forming a monolayer surface coverage, with no interactions between molecules adsorbed. The Langmuir model can be described by the equation: $a = a_m K c_e/(1 + K c_e)$, where a (mmol g^{-1}) and c_e (mmol L^{-1}) are the equilibrium concentration of adsorbate on an adsorbent surface and the adsorbate concentration in solution, respectively. The constant K is the equilibrium constant that represents the affinity between adsorbate and adsorbent and a_m is the maximum amount adsorbed on surface (mg m^{-2}) [21]. The Freundlich model can be expressed by the equation: $a = K c_e{}^{1/p}$ in which K is the equilibrium constant and p is a power parameter. The Freundlich model does not show a saturation of adsorbent surface, the adsorbed amount increases indefinitely with the concentration in solution. The Langmuir–Freundlich isotherm is simple generalization of both isotherms [22]. It makes a good description of adsorption kinetics with adsorption binding interaction among adsorbents molecules. The equation for this isotherm is: $a = a_m (K c_e)^r/[1 + (K c_e)^r]$, where c_e is the adsorbate concentration in equilibrium, K is the affinity constant that includes contribution from surface binding to monomer, monomer–dimer, and more highly associated forms of proteins. The Langmuir–Freundlich coefficient number r represents the cooperativity present in the binding interaction ($r = 1$ represents no interacting site, $r > 1$ a positive cooperativity and $0 < r < 1$ a negative cooperativity) and a_m represents the maximum binding sites or amount of protein adsorbed if each available adsorption site is occupied by a protein molecule [21]. It is known that there are dimmers and hexamers of BSA on aqueous solutions and this quaternary structure is probably involved during the adsorption process at high concentration [4].

For all phosphate or acetate buffers concentrations used in this work, the adsorption process did not follow a typical Langmuir equation as observed elsewhere [19], probably because the adsorption process involved protein-protein interactions. For 0.01 M

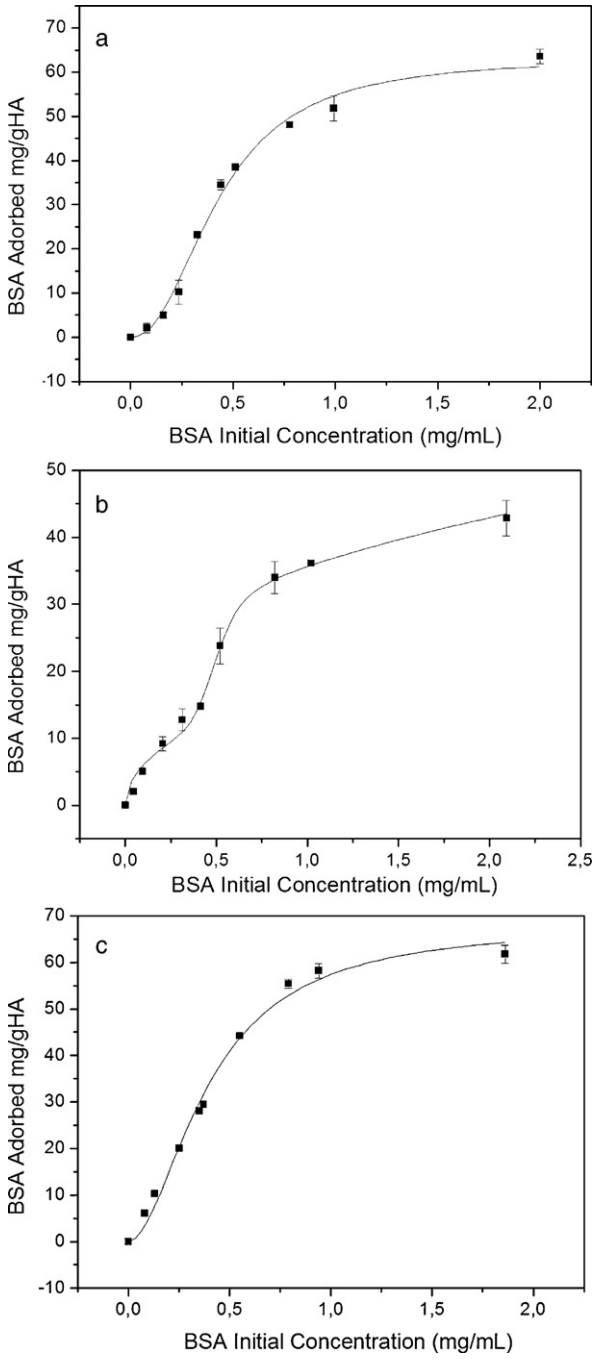

Fig. 2. Isotherms simulation using Langmuir–Freundlich equation for (a) phosphate 0.01 M and (b) acetate 0.01 M; isotherm simulation using the sum of Langmuir and Langmuir–Freundlich equations for (c) phosphate 0.05 M.

buffer concentration – phosphate or acetate – a good agreement to the data points was obtained by fitting the adsorption isotherms with a Langmuir–Freundlich equation as shown in Fig. 2a and b and Table 1. The nature of buffer did not influence the adsorption efficiency (a_m and K parameters). The positive values of r higher than unity indicated the existence of a positive cooperativity in the protein–protein interaction. The increase of the buffer concentration induced an enhancement of the cooperative interaction between BSA molecules and a decrease of the maximum adsorption sites. This behavior could be explained by the competition between phosphate groups (buffer) and COOH groups from BSA for HA surface sites as showed by Wessel et al. [19] and Yin et al. [18].

Table 1
Simulation results of the adsorption isotherms fitting.

Buffer	a_m* (mg/m^2)	K** (mg/mL)	r***	$(1/p)$****
Acetate 0.01 M (Langmuir–Freundlich)	1.51 ± 0.08	2.50 ± 0.2	1.83 ± 0.21	–
Phosphate 0.01 M (Langmuir–Freundlich)	1.41 ± 0.06	2.31 ± 0.13	2.22 ± 0.22	–
Phosphate 0.05 M				
1° step-(Langmuir–Freundlich)	0.39 ± 0.06	2.00 ± 0.09	7.87 ± 3.22	–
2° step-(Freundlich)	–	18.32 ± 2.12	–	2.08 ± 0.23

* a_m (maximum binding sites or amount of protein adsorbed).
** K (equilibrium constant).
*** r (Langmuir–Freundlich coefficient number).
**** p (power of Freundlich equation).

The maximum binding sites and the affinity constant (a_m = 1.5 mg/m^2 and K = 2.5 mL/mg, considering HA BET area of 45 m^2/g) of the HA used in this work were higher than those obtained by Wassel et al. [19] (a_m = 0.62 mg/m^2 and K = 0.15 mL/mg) using a calcium deficient HA with specific surface area of 26 m^2/g and a Langmuir fitting. The higher values of a_m and K parameters verified in this work may be explained by the composition and stoichiometry of the HA surface. The BSA adsorption on

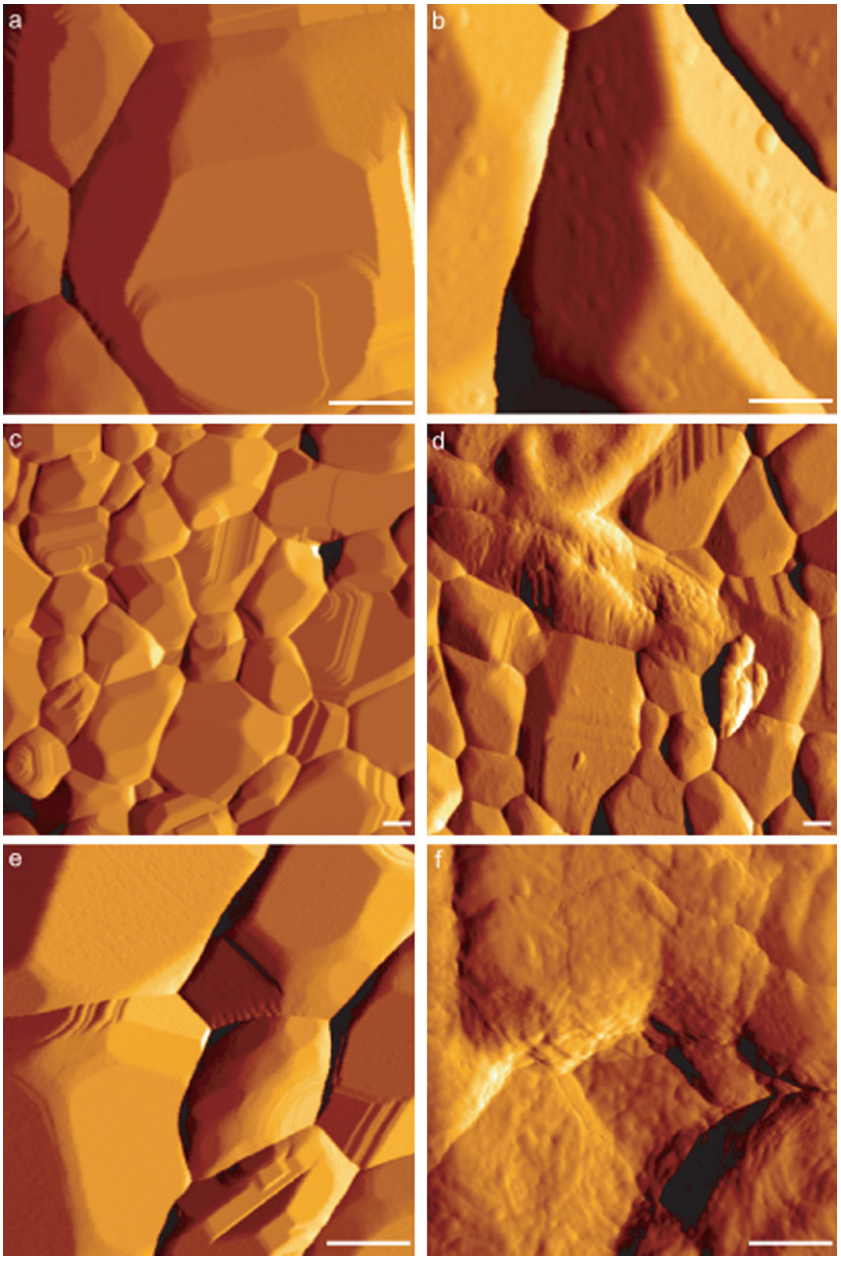

Fig. 3. AFM amplitude signal images before and after BSA adsorption on HA discs. (a) before and (b) after 24 h adsorption with 0.05 mg/mL BSA in phosphate buffer 0.05 M at 3.0 μm × 3.0 μm zoom, (c) before and (d) after 24 h adsorption with 2.0 mg/mL BSA in phosphate buffer 0.05 M at 3.0 μm × 3.0 μm zoom and (e) before and (f) after 24 h adsorption with 2.0 mg/mL BSA in phosphate buffer 0.05 M at 1.0 μm × 1.0 μm zoom (bar = 200 nm).

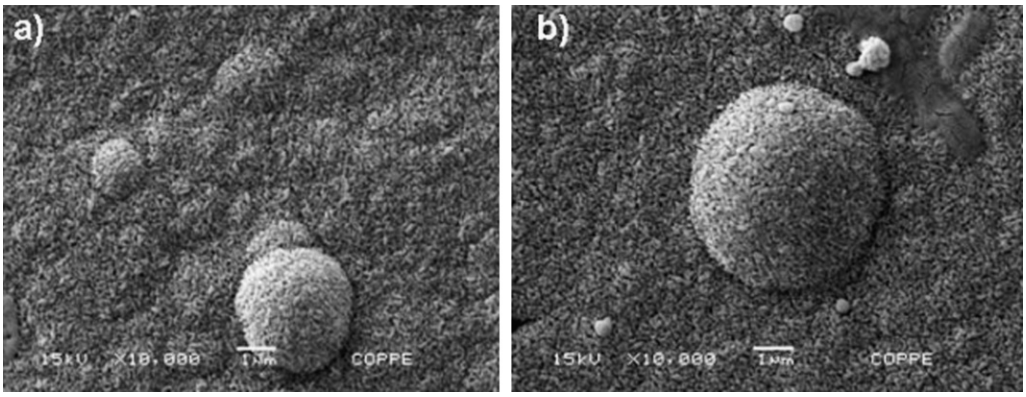

Fig. 4. Scanning electron micrographs of HA disc samples: (a) without BSA after 7 days in n-SBF and (b) with BSA coating after 7 days in n-SBF, 10 K.

HA showed a complex kinetics pattern when phosphate buffer increased to 0.05 M. In this condition the data points could not be fitted by a single equation for all protein initial concentrations. As shown in Fig. 2c the best simulation was achieved by using a Langmuir–Freundlich equation for BSA concentration below 0.4 mg/mL and a pure Freundlich equation for BSA concentration above 0.4 mg/mL. Some conclusions could be taken from these results: (i) the increase of buffer concentration leads to a decrease in adsorption and binding affinity, (ii) a typical Langmuir behavior, associated to a protein monolayer formation and a HA surface with homogeneous distributed sites was not found, (iii) the occurrence of a Langmuir–Freundlich mechanism suggested the existence of cooperative protein-protein interaction on HA surface even for low concentration of BSA, (iv) at high protein concentration the interaction between BSA molecules predominated at HA surface. Many aspects might be considered to understand the non-typical Langmuir adsorption process obtained in this work. One aspect is the heterogeneity of protein surface and its molecular shape that brings to a multiplicity of possible interactions between protein and surface. For example, proteins that possess the ellipsoidal shape two types of orientation of adsorbed molecules may occur: side- and end-on adsorption if major axis is parallel and perpendicular to solid surface, respectively [23]. Conformational change or change in lateral interaction may run concurrently with the adsorption process. Discontinuities in the adsorption isotherms as observed in this work may indicate different concentration-dependent orientation of adsorbed molecules at interface due to a non-spherical protein shape [24].

The ability of BSA to establish strong molecule-molecule interaction when in contact with HA surface was confirmed by AFM analyses performed in sintered discs (1 cm^2 in diameter) before and after the protein adsorption. For BSA initial concentration of 0.05 mg/mL with 24 hours incubation time, the AFM images revealed a thin BSA film covering the HA disc surface still maintaining visible the HA grain boundaries (Fig. 3b). The protein was homogenously distributed over the HA disc surface but small aggregates of protein could be detected at grains surface. The adsorption pattern changed drastically when higher BSA concentrations were used (2.0 mg/mL). In that case, the adsorption was not homogeneous and large aggregates of protein were formed in different parts of discs surface as shown in Fig. 3d and f. These agglomerates can be produced when surface coverage exceeds a saturation value as suggested by Xu et al. [14].

5.2. The reactivity of HA and HA + BSA surface

The reactivity of HA + BSA surface was evaluated by its capability to induce the crystallization of a new calcium phosphate when the surface was in contact with a simulating body fluid solution (n-SBF). For this evaluation, HA discs were coated with a high BSA concentration (1.42×10^{-6} mmol/cm^2) in order to cover the whole HA surface with protein layers and to promote a strong protein–protein interaction on HA surface. In such condition the stability of BSA film on HA surface was assured for periods up to 7 days.

After 7 days soaking in n-SBF, HA discs with BSA (HA + BSA/SBF) and without BSA (HA/SBF) were both fully covered by a thick layer of crystalline particles as observed by SEM, Fig. 4a and b. That thick layer was further characterized as a poorly crystalline calcium phosphate phase (CaP) by FTIRM-ATR and GIXRD measurements. The new layer presented similar crystal morphology in discs with and without BSA. In order to investigate the influence of BSA on the formation of the apatite layer the precipitation rate of calcium and phosphorous onto discs surface were followed by ICP. As shown in Fig. 5, calcium and phosphorous concentration on n-SBF solution decreased gradually with time confirming the precipitation of a new calcium phosphate on HA and HA + BSA discs surface. However, calcium precipitation from SBF solution onto HA + BSA discs was more intense than onto HA discs without BSA while phosphorus concentration decreased equally for HA + BSA and HA discs. Two reasons could explain this effect: (i) BSA layer isolated the HA surface from n-SBF solution and (ii) the affinity of BSA to calcium ions. In the first case the inhibition of calcium dissolution from HA surface by the BSA layer reduced the coprecipitation of the new calcium phosphate coating layer. The BSA layer acted as I shield against HA surface dissolution, reducing the precipitation of the new bioactive calcium phosphate phase. The affinity of BSA with calcium ions by the charged amino acids residues of the protein might also contribute to the difference on calcium precipitation in favor of HA + BSA discs [25,26].

The structure of discs surface with and without BSA, before and after incubation in n-SBF, were characterized by GIXRD using

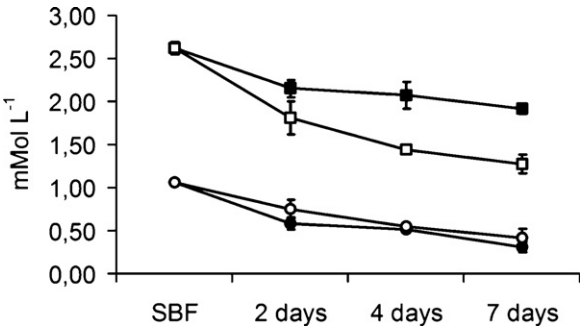

Fig. 5. Calcium and phosphorus content by ICP for HA discs after immersion in n-SBF for 7 days. HA discs uncoated with BSA: Ca (■) and P (●); HA discs coated with BSA: Ca (□) and P (○).

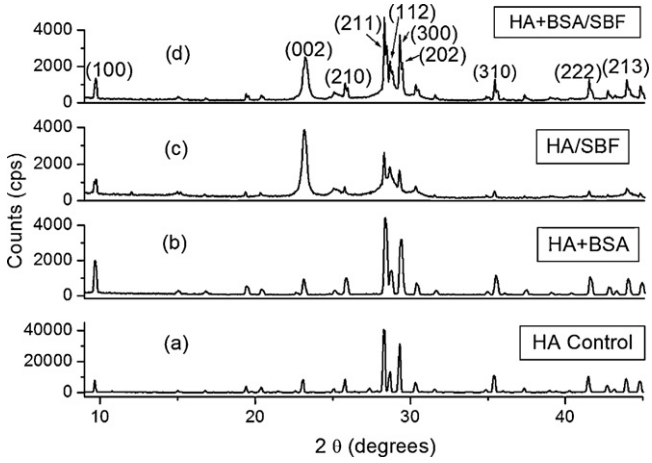

Fig. 6. Low incidence angle XRD pattern of (a) HA disc-control, (b) HA + BSA, (c) HA/SBF and (d) HA + BSA/SBF after immersion in n-SBF for 4 days.

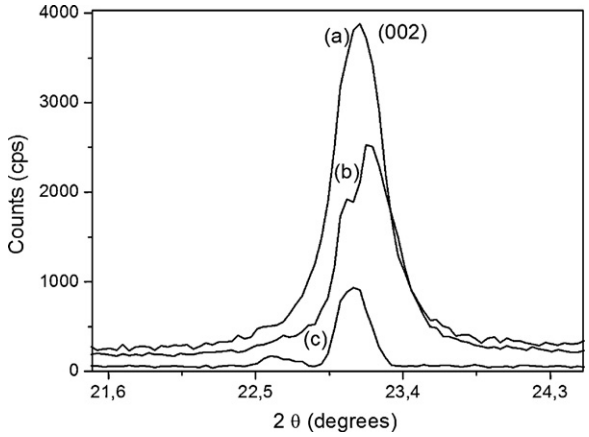

Fig. 7. Low incidence angle XRD pattern of (0 0 2) diffraction peak: (a) HA/SBF, (b) HA + BSA/SBF after immersion in n-SBF for 4 days, and (c) HA + BSA.

9 keV X-rays and an incidence angle of $\theta = 1^\circ$ (HA disc, control) and $\theta = 0.5^\circ$ (for all other samples). In such conditions the penetration depth of X-rays into HA (density of 3.16 g/cm^3) was about 800 nm. The GIXRD analysis of discs before incubation in n-SBF exhibited a XRD pattern with strong and thin peaks. Peaks position and peaks linewidths corresponded to a well-crystallized hydroxyapatite (JCPDS 09-0432), as shown in Fig. 6a and b. The axial pressing and sintering used to process HA discs induced changes on the relative intensities of (2 1 1), (1 1 2), (3 0 0) peaks, Fig. 6a and b.

The GIXRD patterns of HA sample after 4 days incubation in n-SBF, HA/SBF, showed significantly changes in respect to non-treated sample, Fig. 6c. Peaks intensity due to HA substrate decreased dramatically indicating that X-rays beam was mostly adsorbed by the new layer precipitated onto HA surface, as revealed the SEM analyses. The GIXRD pattern of HA/SBF was composed by broad peaks from the new layer and thin peaks from the HA substrate, both located at the same θ position. Therefore, the new compound could be also attributed to a HA phase with a more disordered structure than the substrate. In addition, the crystalline order of the new HA phase had a strong preferential orientation along HA *c* axis because (0 0 2) peak was more intense than (2 1 1, 100%), (3 0 0, 60%) and (2 1 1, 60%). This behavior was characteristic of needle shape particles with crystal growth along the HA *c* direction. That crystalline preferential orientation along the surface was also observed in nanometric thin films of HA deposited onto silicon substrates [27].

After 4 days incubation in n-SBF, sample HA + BSA/SBF also showed a GIXRD pattern composed of thin peaks due to the disc substrate and broad peaks from a low crystalline coating layer precipitated during the contact with SBF solution, Fig. 6d. As already observed in sample HA/SBF, the broad peaks and thin peaks due to HA substrate had the same Θ position. This effect was illustrated in Fig. 7: while the positions of (0 0 2) peaks were coincident for the three samples, HA + BSA/SBF and HA/SBF presented larger (0 0 2) linewidths than HA/BSA. This lead to the conclusion that the precipitated layer on HA + BSA/SBF disc was also formed by a low crystalline HA, as in case of HA discs after n-SBF soaking.

However, some differences between the GIXRD patterns of HA + BSA/SBF and HA/SBF could be observed. First of all, the substrate reflections, (2 1 1), (1 1 2) (3 0 0) and (2 0 2), were more intense in sample HA + BSA/SBF than in sample HA/SBF, as shown in Fig. 6c and d. This effect was attributed to the reduction of the coating layer thickness when BSA was previously bound onto disc surface. Since the precipitated layer became thinner, the X-ray tends to penetrate more deep into the disc surface promoting an enhancement of GIXRD substrate peaks. Second, the GIXRD pattern of HA + BSA/SBF coating layer also showed a preferential orientation along (0 0 2). However, this preference for particle crystallization along c direction was not so pronounced as in case of HA disc without the protein. GIXRD analyses also revealed that a poorly crystalline HA was also formed onto disc surface previously adsorbed with a layer of BSA. On the other hand, the protein acted as a protection layer against HA dissolution and coprecipitation processes, leading to an inhibition of the precipitation rate of the new coating layer.

One interesting finding revealed by the GIXRD analyses was that HA + BSA and HA + BSA/SBF substrates presented HA diffraction patterns corresponding to two HA structures while a unique HA phase was associated to HA/SBF substrate, Fig 8.. The existence of double GIXRD patterns indicated that the most superficial layer of the HA disc (thickness < 800 nm) had cell parameters slightly different from the interior. In this case the GIXRD pattern is constituted by two contributions: (i) from the disc interior and (ii) from a superficial layer located just beneath the disc surface. In a conventional XRD measurement with Cu kα radiation it is not possible to identify peaks from surface phase because reflections from the disc interior dominate. When GIXRD is performed with a high intensity beam from synchrotron radiation the surface contribution is enhanced and small changes in the structure of nanometric surface layers

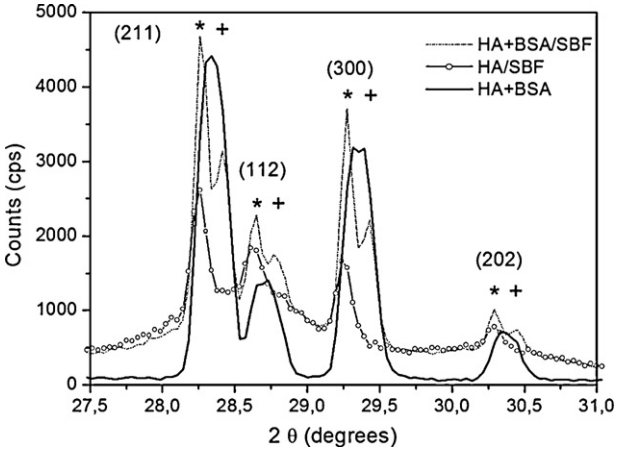

Fig. 8. Low incidence angle XRD pattern of HA + BSA (solid line); HA/SBF (solid line + ○) and HA + BSA/SBF (short dash) after immersion in n-SBF for 4 days. HA peaks of (*) substrate interior and (+) strained surface layer corresponding to (2 1 1), (1 1 2), (3 0 0) and (2 0 2) planes in $28^\circ < 2\Theta < 31^\circ$ region.

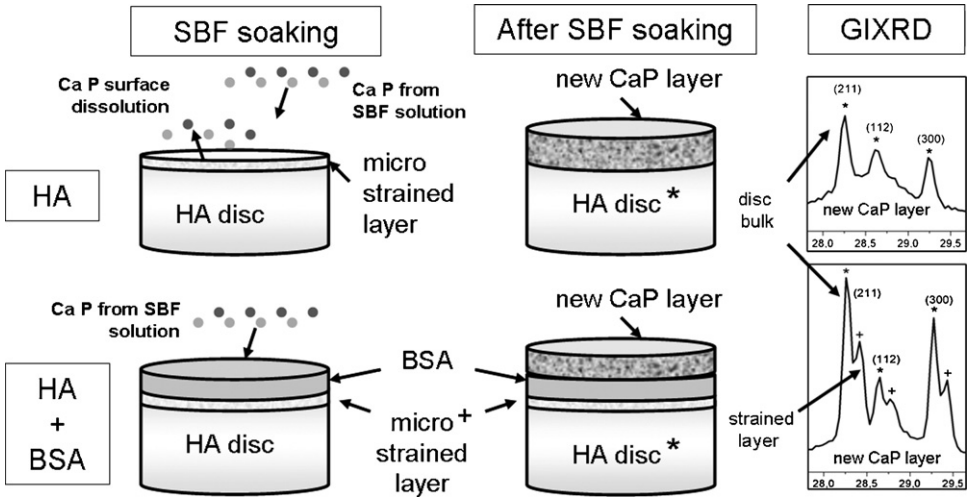

Fig. 9. Schematic diagram illustrating the HA and the HA + BSA surfaces before and after the simulated body solution (SBF) soaking. BSA adsorbed onto the HA surface shields the strained surface layer during the SBF soaking decreasing the precipitation of the new CaP phase. The GIXRD peaks from disc bulk, strained layer and new CaP phases are shown in the diffractions pattern of HA/SBF and HA + BSA/SBF.

can be detected. The, mechanical deformations and strains induced at disc surface by processing – uniaxial pressing and sintering – were probably the responsible for the superficial layer with unit cell parameters slightly different from the bulk [28].

The existence of one phase in the GIXRD pattern of HA/BSA substrate, Fig. 8 could be attributed to the dissolution of the strained surface layer during the incubation in SBF for 4 days. This dissolution contributed for the precipitation of the CaP coating layer as was discussed previously. A different situation occurred when BSA was previously bound to disc surface, as shown in Fig. 8. In that case the GIXRD pattern of the strained layer was still detected after 4 days incubation in SBF indicating that BSA acted as an isolating layer, inhibiting the HA surface dissolution.

The diagram of Fig. 9 summarizes the previous conclusions concerning the formation of the new calcium phosphate layer (CP) onto HA surface with and without BSA when discs are in contact with a simulated body solution. As shown in Fig. 9, calcium and phosphate ions from SBF and from surface dissolution contribute to the supersaturation condition that is a necessary for CP precipitation onto HA surface. When BSA is bound onto HA surface the release of Ca and P from dissolution is blocked and supersaturation condition is not so favorable. As consequence, the efficiency of CP precipitation tends to be lower when compared to HA surface without the protein.

FTIRM-ATR microscopy was used to obtain additional information concerning the binding of BSA onto HA surface and the nature of the calcium phosphate layer precipitated onto discs during the incubation in Milli-Q water and n-SBF. This technique was sensitive to detect vibrational spectra from ionic groups located in a surface layer of HA discs within 3 μm in thickness. The FTIRM-ATR spectra of HA discs after incubation in water, Fig. 10, showed straight bands at 1087 cm^{-1}, 1062 cm^{-1}, 1006 cm^{-1} and 959 cm^{-1} that were attributed to phosphate groups in crystalline apatite environment [29]. The band at 1006 cm^{-1}, not usual in powder HA, could be attributed to changes in phosphate vibrational modes due to surface micro-strain induced by axial press and discs sintering. This aggressive treatment could affect the vibration modes of phosphate groups and the FTIRM-ATR band positions as also observed by Zeng et al. [30].

The FTIRM-ATR spectra of HA + BSA presented phosphate bands of HA substrate and bands due to amide I and II groups of BSA, Fig. 11. According to the literature intense interactions with surfaces can change the protein conformation or induce protein denaturation [31]. The position of amide I band is frequently used

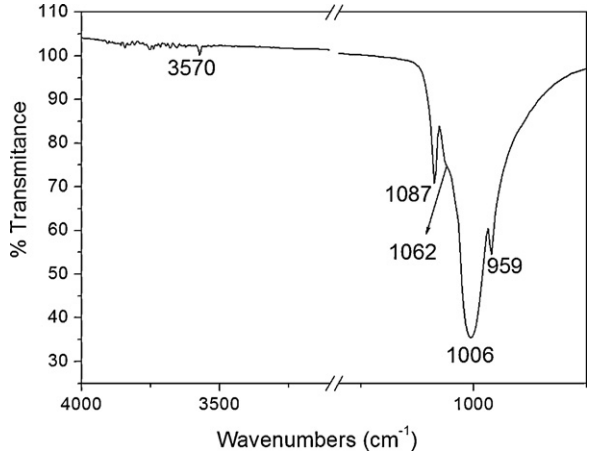

Fig. 10. FTIRM-ATR spectra of HA disc after immersion in Milli-Q water for 1 day.

to monitor conformational changes on proteins during adsorption process [32], which could affect protein biological activity [33]. In this work, the BSA amide I vibrations were observed at 1686 cm^{-1} and 1645 cm^{-1} whereas the native BSA alpha-helix bands, which

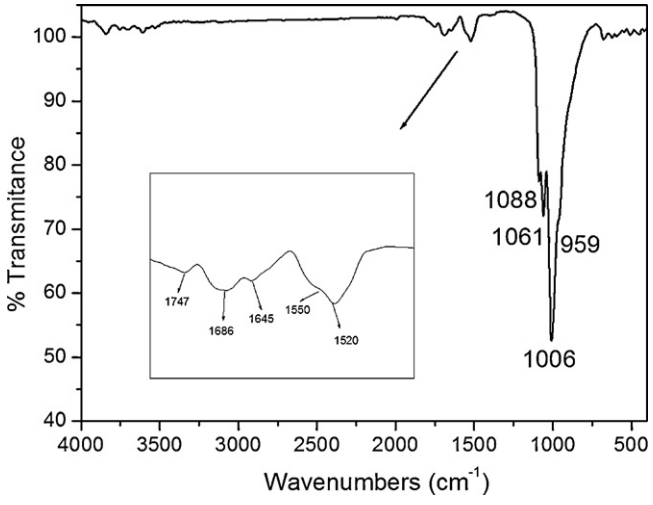

Fig. 11. FTIRM-ATR spectra of HA + BSA.

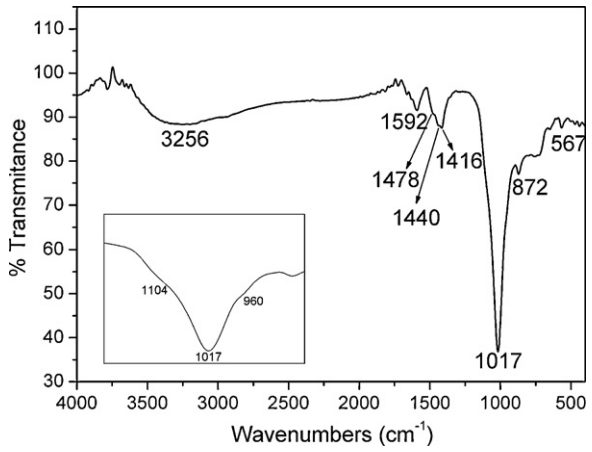

Fig. 12. FTIRM-ATR spectra of HA/SBF after immersion in n-SBF for 7 days.

correspond to the main secondary structure of the protein usually occur at 1660–1650 cm^{-1} [34]. This change in amide I bands position indicated that interaction with HA surface induced strong changes in BSA conformational state in favor of less-ordered conformations [32]. The amide II bands due to N–H bending and C–N stretching vibrations were observed in the same position (1550 cm^{-1}) as amide II band of native BSA. However, an additional band at 1520 cm^{-1} could be attributed to an interaction between N–H and positive charged sites (calcium sites) of HA surface.

The FTIRM-ATR spectra of HA and HA + BSA discs after the immersion in n-SBF for 7 days (Figs. 12 and 13) differed from those of non-treated discs (Figs. 10 and 11). Phosphate bands in the 900–1200 cm^{-1} region were broad confirming the XRD results that the new phase precipitated onto HA surface was poorly crystalline calcium phosphate. As shown in Fig. 12, HA/SBF sample showed a very intense phosphate band centered at 1017 cm^{-1} with shoulders at 1104 cm^{-1} and 960 cm^{-1}. These bands are characteristics of PO_4^{3-} and HPO_4^{2-} in calcium deficient HA. Carbonate bands at 872 cm^{-1}, 1416 cm^{-1}, 1440 cm^{-1} and 1478 cm^{-1} indicated that a carbonated HA was precipitated onto the disc surface. The 1592 cm^{-1} band was characteristic for water associated with HA [29]. FTIRM-ATR spectrum of HA + BSA/SBF, Fig. 13, presented phosphate band centered at 1019 cm^{-1} with shoulders at 1099 cm^{-1} and 958 cm^{-1}. These bands were assigned to PO_4^{3-} and HPO_4^{2-} in calcium deficient HA. The carbonate bands were also present at 872 cm^{-1} and 1419 cm^{-1}, with small bands at 1445 cm^{-1} and 1478 cm^{-1}, confirming that n-BSA layer onto HA surface was also capable to induce a carbonated apatite coating onto the disc surface.

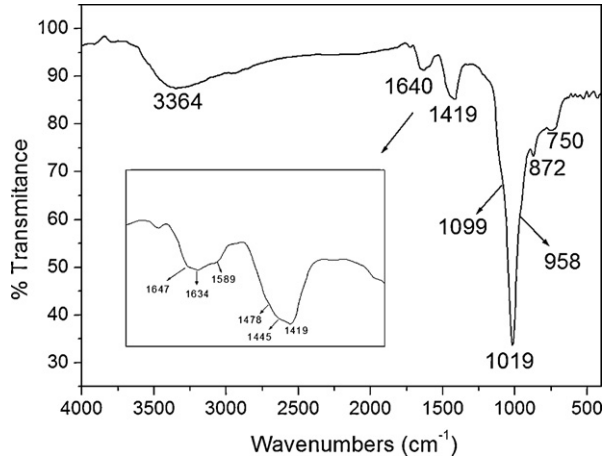

Fig. 13. FTIRM-ATR spectra of HA + BSA/SBF after immersion in n-SBF for 7 days.

6. Conclusion

Albumin was strongly adsorbed on HA surface and remained bounded to the surface up to 7 days of immersion in n-SBF. The BSA binding affinity to HA surface decreased with the increase of phosphate buffer concentration. No significant change in BSA adsorption was verified when the experiment was performed in the 0.01 M acetate buffer concentration. The BSA sorption onto HA surface, even for low BSA concentration, did not follow a Langmuir behavior that involves the formation of a monolayer of non-interacting proteins. The occurrence of Langmuir–Freundlich mechanisms for all protein concentrations indicated the existence of strong cooperative protein–protein interactions on HA surface. These strong interactions enhanced the formation of protein aggregates on HA surface as could be verified by AFM analyses. The GIXRD analysis combined with FTIRM-ATR spectroscopy showed that BSA coating promoted the precipitation of a poorly crystalline carbonated hydroxyapatite on HA surface with preferential crystal growth along apatite c axis direction. However, the *in vitro* bioactivity of HA surface coated with BSA was reduced in comparison to the uncoated surface. The explanation for this reduction was based in the proposal that the new apatite layer was formed by two contributions: the precipitation of calcium and phosphorus from SBF and the dissolution of the apatite surface. When the protein layer was bound to the HA surface the second contribution was reduced, leading to a decrease of the calcium phosphate precipitation.

Acknowledgements

The authors would like to thank CNPq and FAPERJ for the financial support, Marcia Sader and Prof. Gloria A. Soares (Department of Materials and Metallurgical Engineering/COPPE/UFRJ) and Valeria C. A. Moraes (Brazilian Center for Physical Research) for SEM and XRD analyses.

References

[1] W. Kaim, B. Schwederski, Bioinorganic Chemistry: Inorganic Elements in the Chemistry of Life- An Introduction and Guide, John Wiley & Sons, 1994.
[2] R. Rohanizadeh, M. Padrines, J.M. Bouler, D. Couchourel, Y. Fortun, G. Daculsi, J. Biomed, Mater. Res. 42 (1998) 530–539.
[3] Z. Schwartz, B.D. Boyan, J. Cell. Biochem. 56 (1994) 340–347.
[4] C. Combes, C. Rey, Biomaterials 23 (2002) 2817–2823.
[5] P. Ducheyne, Q. Qiu, Biomaterials 20 (1999) 2287–2303.
[6] S.A. Bender, J.D. Bumgardner, M.D. Roach, K. Bessho, J.L. Ong, Biomaterials 21 (2000) 299–305.
[7] A.L. Boskey, J. Cell. Biochem. Supplements 30/31 (1998) 83–91.
[8] M.C. Coen, R. Lehmann, P. Groning, M. Bielmann, C. Galli, L. Schlapbach, J. Colloid Interface Sci. 233 (2001) 180–189.
[9] S. Sharma, G.P. Agarwal, An. Biochem. 288 (2001) 126–140.
[10] Y. Wang, S. Zhang, X. Zeng, K. Cheng, M. Qian, W. Weng, Mater. Sci. Eng. 27 (2007) 244–250.
[11] P.A.A.P. Marques, S.C.P. Cachinho, M.C.F. Magalhães, R.N. Correia, M.H.V. Fernandes, J. Mater. Chem. 14 (2004) 1861–1866.
[12] E. Mueller, C.S. Sikes, Calcif Tissue Int. 52 (1993) 34–41.
[13] E.D. Eanes, H.I. Gillessen, A.S. Posner, Nature 23 (1965) 365–367.
[14] T. Xu, R. Fu, L. Yan, J. Colloid Interface Sci. 262 (2003) 342–350.
[15] H. Urano, S. Fukuzaki, J. Biosci. Bioeng. 90 (1) (2000) 105–111.
[16] A. Kondo, S. Oku, K. Higashitani, J. Colloid Interface Sci. 143 (1991) 214–221.
[17] T. Kokubo, H. Takadama, Biomaterials 27 (2006) 2907–2915.
[18] G. Yin, Z. Liu, J. Zhan, F. Ding, N. Yuan, Chem. Eng. J. 87 (2002) 181–186.
[19] D.T.H. Wassell, R.C. Hall, G. Embery, Biomaterials 16 (1995) 697–702.
[20] G. Yin, Z. Liu, J. Zhan, F. Ding, N. Yuan, Chem. Eng. J. 87 (2002) 181–186.
[21] P. Praus, M. Turicová, J. Braz. Chem. Soc. 18 (2007) 378–383.
[22] R. Sips, J. Chem. Phys. 18 (1950) 1024–1026.
[23] H. Terashima, T. Tsuji, Colloids Surf. B: Biointerfaces 27 (2002) 115–122.
[24] S. Oscarsson, J. Chromatogr. B 699 (1997) 117–131.
[25] A. Besarab, A. Deguzman, J.W. Swanson, J. Clin. Pathol. 34 (1981) 1361–1367.
[26] D.E. Fleming, W. Van Bronswijk, R.L. Ryall, Clin. Sci. 101 (2001) 159–168.

[27] A. Mello, E. Mavropoulos, Z. Hong, J.B. Ketterson, A.M. Rossi, Key Eng. Mater. 396–398 (2009) 369–372.
[28] B.D. Cullity, Elements of X-Ray diffraction, Addison-Wesley Publishing Company, 1978.
[29] S. Koutsopoulos, J. Biomed. Mater. Res. 62 (2002) 600–612.
[30] H. Zeng, W.R. Lacefield, Biomaterials 21 (2000) 23–30.
[31] C.S. Lee, G. Beltfort, Proc. Natl. Acad. Sci. U.S.A. 86 (1989) 8392–8396.
[32] P. Roach, D. Farrar, C.C. Perry, J. Am. Chem. Soc. 127 (2005) 8168–8173.
[33] M.C. Coen, R. Lehmann, P. Groning, M. Bielmann, C. Galli, L. Schlapbach, J. Colloid Interface Sci. 233 (2001) 180–189.
[34] H. Zeng, K.K. Chittur, W.R. Lacefield, Biomaterials 20 (1999) 377–384.